Optically trapping Rayleigh particles by using focused partially coherent multi-rotating elliptical Gaussian beams

Xi Peng (彭 喜)[1,2], Chidao Chen (陈迟到)[1,2], Bo Chen (陈 波)[1,2], Yulian Peng (彭玉莲)[1,2], Meiling Zhou (周美玲)[1,2], Xiangbo Yang (杨湘波)[1], and Dongmei Deng (邓冬梅)[1,2,*]

[1]*Guangdong Provincial Key Laboratory of Nanophotonic Functional Materials and Devices, South China Normal University, Guangzhou 510631, China*

[2]*CAS Key Laboratory of Geospace Environment, University of Science & Technology of China, Chinese Academy of Sciences, Hefei 230026, China*

**Corresponding author: dmdeng@263.net*

Received June 23, 2015; accepted November 6, 2015; posted online December 18, 2015

By investigating the cross-spectral density of partially coherent multi-rotating elliptical Gaussian beams (REGBs) that propagate through a focusing optical system, we obtain the radiation force on a Rayleigh particle. The radiation force distribution is studied under different beam indexes, coherence widths, and elliptical ratios of the partially coherent multi REGBs. The transverse and the longitudinal trapping ranges can increase at the focal plane by increasing the beam index or decreasing the coherence width. The range of the trapped particle radii increases as the elliptical ratio increases. Furthermore, we analyze the trapping stability.

OCIS codes: 140.3295, 140.7010, 350.5500.

doi: 10.3788/COL201614.011405.

In recent years, light beams with rotating characteristics have attracted quite a lot of interest due to their peculiar properties, which present opportunities for research in the fields of science and technology[1–5]. For example, the ability of rotating beams to rotate particles provides a new degree of control for micrometer-sized particles, and has important applications in optical manipulating and biological specimens rotating. In optics, a more general form of rotating elliptical Gaussian beams (REGBs) are thoroughly studied[1,5–9]. REGBs, which have an elliptical light spot and whose phase front rotates along the propagating axis of the beam, are obtained from an ordinary Gaussian beam[7].

Ashkin and colleagues demonstrated radiation pressure-trapping particles[10–12] in a series of pioneering Letters, through which the "optical trap" came to be known. The optical force has traditionally been decomposed into two components: one is the scattering force, which is in the direction of the light propagation, and the other is the gradient force, which is in the direction of the spatial light gradient[13]. Optical trapping and manipulation of micrometer-sized particles produced by piconewton-level forces while simultaneously measuring displacement with nanometer-level precision have attracted a very wide range of attention[14–18]. Since their invention, optical trapping techniques continue to improve and become better established, and have emerged as a powerful tool with broad-reaching applications in physics and life sciences research[19,20]. Today, many researchers report optical trapping produced by beams such as Gaussian Schell model beams[21], Laguerre–Gaussian beams[22], highly focused Lorentz–Gaussian beams[23], and highly focused, elegant Hermite-cosine-Gaussian beams[24]. In most studies, the incident light beams for optical traps are assumed to be fully coherent[21–24]. As we know, any laser field is always partially coherent in practice[25–28]. In this Letter, the cross-spectral density (CSD) of partially coherent multi-REGBs propagating through a focusing optical system is derived and used to investigate the radiation forces on a Rayleigh particle. Compared to the work in Ref. [16], the radiation force of the partially coherent multi-REGBs can rotate. To trap oval particles, we can adjust the sizes of the forces in some directions by changing the elliptical ratio of the elliptical beams, which ordinary Gaussian beams cannot do. Furthermore, the trapping stability conditions are analyzed.

Under the free-space rectangular coordinates system, the electric field of the REGB in the $z = 0$ plane can be expressed as[1,5]

$$E_0(x', y') = A_0 \exp\left[-\left(\frac{x'^2}{w_x^2} + \frac{y'^2}{w_y^2} + \frac{ix'y'}{R_0}\right)\right], \quad (1)$$

where A_0 is the constant complex amplitude of E_0, w_x and w_y are the initial beam widths on the x- and y-axes, respectively, and R_0 specifies the beam rotation. Without loss of generality, the spectral degree of coherence is given by[29]

$$g(\mathbf{r}_1' - \mathbf{r}_2') = \exp\left[-\frac{(\mathbf{r}_1' - \mathbf{r}_2')^2}{\delta^2}\right], \quad (2)$$

where $\mathbf{r}_1'(x_1', y_1')$ and $\mathbf{r}_2'(x_2', y_2')$ are the original position vectors, and δ is the coherence length. By taking all of the above assumptions into consideration, the CSD of the partially coherent multi-REGBs of the source plane can be written in the Cartesian coordinates as[25]

$$W^0(x_1', y_1', x_2', y_2'; z=0) = \frac{1}{C_0}\sum_{m=1}^{M}\frac{(-1)^{m-1}}{m}\binom{M}{m}E_1^* E_2 g(\mathbf{r}_1' - \mathbf{r}_2')$$
$$= \frac{A_0^2}{C_0}\sum_{m=1}^{M}\frac{(-1)^{m-1}}{m}\binom{M}{m}\exp\left[-\left(\frac{x_1'^2}{w_x^2}+\frac{y_1'^2}{w_y^2}+i\frac{x_1'y_1'}{R_0}\right)-\left(\frac{x_2'^2}{w_x^2}+\frac{y_2'^2}{w_y^2}-i\frac{x_2'y_2'}{R_0}\right)\right.$$
$$\left.-\left(\frac{x_1'^2+x_2'^2-2x_1'x_2'+y_1'^2+y_2'^2-2y_1'y_2'}{2m\delta^2}\right)\right], \quad (3)$$

where $C_0 = \sum_{m=1}^{M}[(-1)^{m-1}/m]\binom{M}{m}$ is the normalization factor with $\binom{M}{m}$ representing the binomial coefficients, and $*$ denotes the complex conjugate.

Considering the propagation of the partially coherent multi-REGBs through an unapertured lens system (see Fig. 1), where z is the distance from the input plane to the output plane, f is the focal length, and z_1 is the axial distance from the focal plane to the output plane, the ABCD matrix for the focusing system is

$$\begin{pmatrix} A & B \\ C & D \end{pmatrix} = \begin{pmatrix} 1 & z \\ 0 & 1 \end{pmatrix}\begin{pmatrix} 1 & 0 \\ -1/f & 1 \end{pmatrix} = \begin{pmatrix} 1-z/f & z \\ -1/f & 1 \end{pmatrix}. \quad (4)$$

Then, the expression for the CSD of the electric field in the output plane is given by[30]

$$W(x_1, y_1, x_2, y_2; z) = \left(\frac{k}{2\pi B}\right)^2 \iiiint \mathrm{d}x_1'\mathrm{d}x_2'\mathrm{d}y_1'\mathrm{d}y_2' W^0$$
$$\times \exp\left\{\frac{ik}{2B}[(Ax_2'^2 - 2x_2'x_2 + Dx_2^2) + (Ay_2'^2 - 2y_2'y_2 + Dy_2^2) - (Ax_1'^2 - 2x_1'x_1 + Dx_1^2) - (Ay_1'^2 - 2y_1'y_1 + Dy_1^2)]\right\}, \quad (5)$$

where λ is the wavelength of the incident light, $k = 2\pi/\lambda$ is the wavenumber in free space, and $\mathbf{r}_1(x_1, y_1)$ and $\mathbf{r}_2(x_2, y_2)$ are the position vectors in the output plane. If we substitute Eqs. (3) and (4) into Eq. (5), performing the related integration, and assume that $\mathbf{r}_1 = \mathbf{r}_2 = \mathbf{r}(x_1 = x_2 = x, y_1 = y_2 = y)$, then the CSD reduces to

$$W(\mathbf{r}, \mathbf{r}; z) = \frac{A_0^2}{\Delta}\frac{1}{C_0}\sum_{m=1}^{M}\frac{(-1)^{m-1}}{m}\binom{M}{m}\exp(Y_1), \quad (6)$$

$$\Delta = \sqrt{\left(A^2 + \frac{4B^2}{k^2}X_1\right)\left(A^2 + \frac{4B^2}{k^2}X_2\right)}, \quad (7)$$

$$X_1 = \left(\frac{1}{w_x^2}\right)^2 + \frac{1}{m\delta^2 w_x^2} - \left(\frac{i}{2R_0}\right)^2, \quad (8)$$

$$X_2 = \left(\frac{1}{w_y^2}\right)^2 + \frac{1}{m\delta^2 w_y^2} - \left(\frac{i}{2R_0}\right)^2, \quad (9)$$

$$Y_1 = -\frac{2}{\Delta^2}\left[\epsilon_x\frac{x^2}{w_x^2} - \frac{2BA}{kR_0}\left(\frac{1}{w_x^2}+\frac{1}{w_y^2}\right)xy + \epsilon_y\frac{y^2}{w_y^2}\right], \quad (10)$$

$$\epsilon_x = A^2 + \frac{4B^2}{k^2}\left[\left(\frac{1}{w_y^2}\right)^2 + \frac{1}{m\delta^2 w_y^2} - \frac{w_x^2}{w_y^2}\left(\frac{i}{2R_0}\right)^2\right], \quad (11)$$

$$\epsilon_y = A^2 + \frac{4B^2}{k^2}\left[\left(\frac{1}{w_x^2}\right)^2 + \frac{1}{m\delta^2 w_x^2} - \frac{w_y^2}{w_x^2}\left(\frac{i}{2R_0}\right)^2\right]. \quad (12)$$

The intensity distribution and the CSD of the partially coherent multi-REGBs at any point of the output plane are related by the formulas[25]

$$I_{\mathrm{out}}(\mathbf{r}; z) = W(\mathbf{r}, \mathbf{r}; z). \quad (13)$$

In this Letter, we choose $f = 0.1$ mm, $\lambda = 1064$ nm, $w_x = 0.6$ mm, $w_y = 0.1$ mm, $R_0 = 1$ m^2, $A_0^2 = 1$ W/mm^2, and $\delta = 0.1$ mm. Figure 2 shows that the beam profile becomes flatter, but the maximum intensity decreases as the beam index M increases (for example, $M = 10$, $M = 30$),

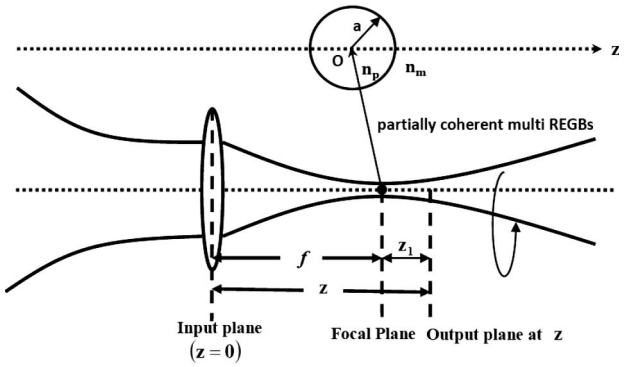

Fig. 1. Schematic of a focusing optical system. a is the radius of the particle, n_p is the refractive index of the particle, and n_m is the refractive index of the ambient.

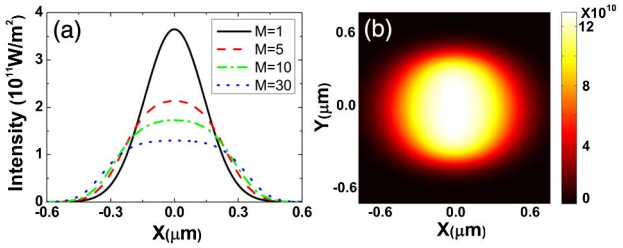

Fig. 2. (a) Intensity distribution for different values of M at the focal plane. (b) Two-dimensional intensity distribution for $M = 30$.

which means the potential wells are lower or shallower than their counterparts (for example $M = 1$, $M = 5$).

We study the radiation force of partially coherent multi-REGBs on a Rayleigh dielectric particle, which is sufficiently small compared with the wavelength (i.e., the particle radius $a \le \lambda/20$) and can be seen as a point dipole in the light field. The scattering force and the gradient force are given by[13,21]

$$\vec{F}_{\text{scat}}(\vec{\mathbf{r}}; z) = \vec{e}_z n_m \alpha_0 I_{\text{out}}/c, \tag{14}$$

$$\vec{F}_{\text{grad}}(\vec{\mathbf{r}}; z) = 2\pi n_m \beta_0 \nabla I_{\text{out}}/c, \tag{15}$$

where $\vec{e}_z$ is a unity vector along the beam propagation, and $\alpha_0 = (128\pi^5 a^6/3\lambda^4)[(m_0^2-1)/(m_0^2+2)]^2$, $\beta_0 = a^3(m_0^2-1)/(m_0^2+2)$, $m_0 = n_p/n_m$ is the relative refraction index of the particle. We choose $a = 40$ nm, $n_p = 1.8$, and $n_m = 1.33$ (water). By substituting Eq. (13) into Eqs. (14) and (15), we can calculate the radiation force induced by partially coherent multi-REGBs on a Rayleigh particle. Both the scattering force and the gradient force will be greatly affected by the beam index M, the coherence width δ, and the elliptical ratio γ ($\gamma = w_x/w_y$); Figs. 3–5 show this numerically.

Figure 3 shows the influence of the beam index M on the radiation force produced by the partially coherent multi-REGBs. From Figs. 3(a), 3(d), and 3(g), we can see that a Rayleigh particle whose refractive index is larger than that of the ambient can be trapped at the focus point by the partially coherent multi-REGBs, because there are stable equilibrium points in Figs. 3(d) and 3(g). From Fig. 3(h), we can see that when $M = 1$, the partially coherent multi-REGBs could not stably trap the particle when $x = 0.3$ μm, because the direction of the longitudinal gradient force is same as the scattering force direction.

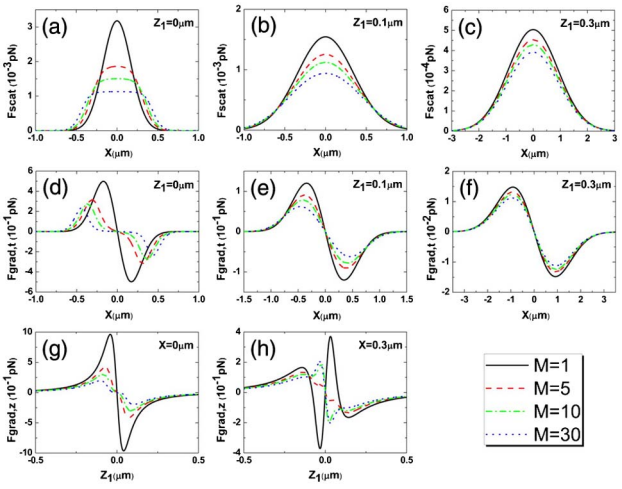

Fig. 3. Effect of the beam index M on (a)–(c) F_{scat} (the scattering force), (d)–(f) $F_{\text{grad},t}$ (the transverse gradient force). $F_{\text{grad},t} = (F_{\text{grad},x}^2 + F_{\text{grad},y}^2)^{1/2}$ while $z_1 < 0$; $F_{\text{grad},t} = -(F_{\text{grad},x}^2 + F_{\text{grad},y}^2)^{1/2}$ while $z_1 > 0$. (g) and (h) The effect of the beam index on $F_{\text{grad},z}$ (the longitudinal gradient force). The parameters are chosen as $y = 0$ and $\delta = 0.1$ mm.

But for larger M ($M = 5, 10, 30$), the direction of the longitudinal gradient force is against to the direction of the scattering force. So we can conclude that by increasing the beam index M of the partially coherent multi-REGBs, we can increase the transverse trapping range at the focal plane. By comparing the figures in Fig. 3, one can find that both the gradient force and the scattering force decrease as the initial beam index M increases, which means that the trapping stability changes.

Figure 4 shows the influence of the coherence width δ on the radiation force produced by the partially coherent multi-REGBs. From Figs. 4(d) and 4(g), we find that at the focal plane, as the coherence width of the partially coherent multi-REGBs decreases, the positions of the peak values deviate away from the focus point. This means that both the transverse and the longitudinal trapping ranges become larger. However, as is shown in Fig. 4(h), the direction of the longitudinal gradient force will reverse when the coherence width increases to 0.2 mm at $x = 0.3$ μm, and the beam will lose the ability to trap the particle. By decreasing the coherence width δ of the partially coherent multi-REGBs, we can increase the trapping ranges. One can see from Fig. 4 that the scattering force and the transverse and the longitudinal gradient forces decrease as the coherence width of the initial partially coherent multi-REGBs decreases. Partially coherent beams have their advantages when trapping.

Figure 5 shows the influence of the elliptical ratio γ on the radiation force produced by the partially coherent multi-REGBs. From Fig. 5, we can see that both the gradient force and the scattering force increase as the elliptical ratio γ increases, which means that the trapping stiffness is higher. The positions of the peak value deviate away from the focus point as γ increases, as shown in the Figs. 5(e) and 5(f). As γ increases, the trapping range broadens, demonstrating the advantage of using elliptical beams. From Figs. 5(a), 5(d), and 5(g), we can see that a Rayleigh particle can be trapped at the focus point by the

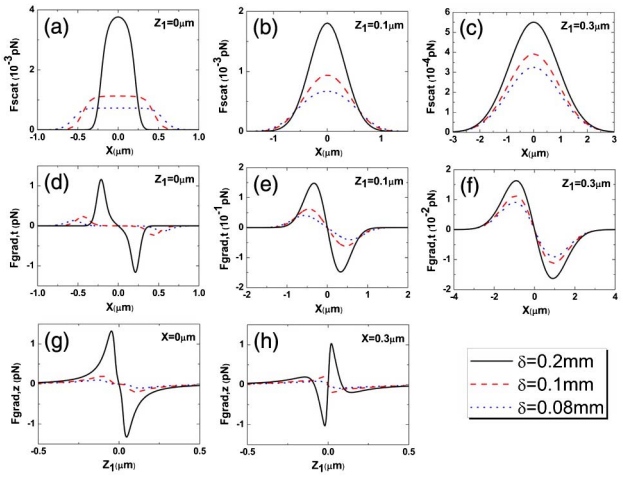

Fig. 4. Effect of the coherence width δ on (a)–(c) F_{scat}, (d)–(f) $F_{\text{grad},t}$, and (g) and (h) $F_{\text{grad},z}$. The parameters are chosen as $y = 0$, $M = 30$.

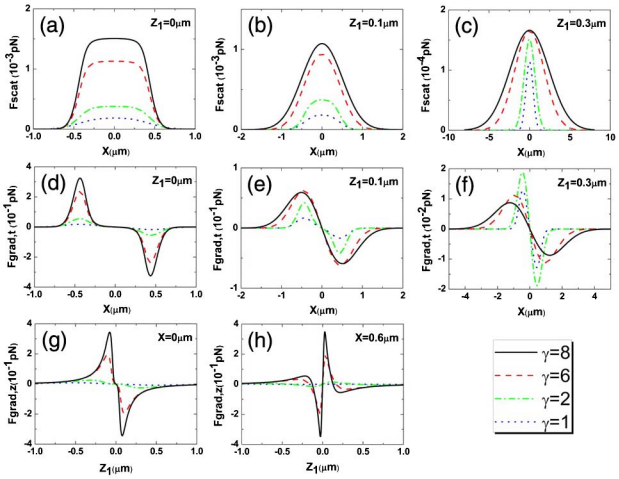

Fig. 5. Effect of the elliptical ratio γ on (a)–(c) F_{scat}, (d)–(f) $F_{\mathrm{grad},t}$, and (g) and (h) $F_{\mathrm{grad},z}$. The parameters are chosen as $y = 0$, $M = 30$, $\delta = 0.1$ mm, and $w_y = 0.1$ mm.

partially coherent multi-REGBs because there are stable equilibrium points in Figs. 5(d) and 5(g) for different values of γ. For the oval particles, we can adjust the size of forces in all directions by changing the elliptical ratio of elliptical beams, which ordinary Gaussian beams ($\gamma = 1$) cannot do. So when we choose different values of γ, we can

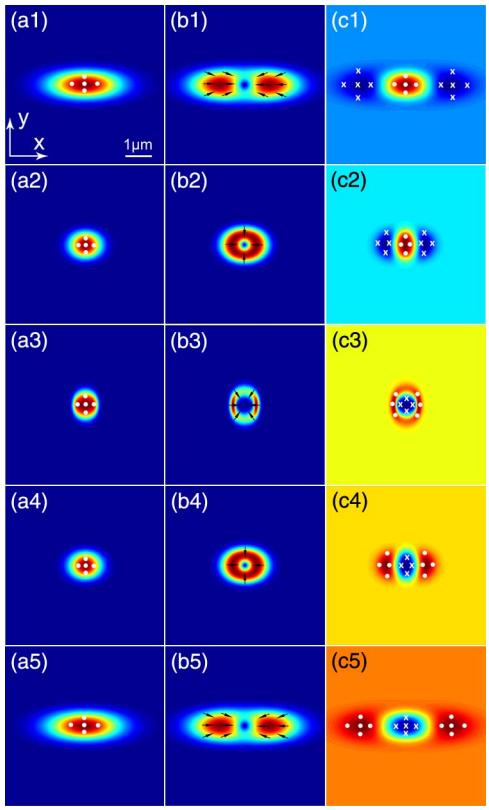

Fig. 6. Two-dimensional force distribution of the REGBs near the focus point. (a1)–(a5) are the scattering force distributions. (b1)–(b5) are the transverse gradient force distributions. (c1)–(c5) are the longitudinal gradient forces distributions at positions $z_1 = -0.3$, -0.1, 0, 0.1, and 0.3 mm.

get the different trapping ranges, which is beneficial for the application.

For stable trapping, the gradient force must be large enough to overcome the scattering force $R = |F_{\mathrm{grad},z}|/|F_{\mathrm{scat}}| \geq 1$, where the ratio R is called the stability criterion. As is shown in Figs. 3–5, the scattering force is much smaller than the longitudinal gradient force near the focal plane. Figure 6 shows the two-dimensional force distribution of the partially coherent multi-REGBs near the focus point. In this process, the direction of the scattering force is always along the z direction (white points indicate the $+z$ direction and white forks indicate the $-z$ direction), and the direction of the transverse gradient force always points to the center of the beam (arrows). But the direction of the longitudinal force will change when the beams pass through the focus plane. As the direction of the transverse force always points to the center of the beam, the particle can be trapped stably in transverse direction. When $z_1 > 0$, the particle can be trapped stably in longitudinal direction, as the direction of the scattering force and the center of the longitudinal force are opposite. The partially coherent multi-REGBs rotate while propagating, and the force scope changes. The rotational nature of these beams is interesting for the rotating trapped particle.

The Brownian force, which describes the influence of the Brownian motion, can be calculated by the expression[31]

$$|F_b| = \sqrt{12\pi\eta a K_B T}, \tag{16}$$

where η is the viscosity of the ambient, which is 8.0×10^{-4} Pa · s at $T = 300$ K, a is the radius of the Rayleigh particle, and K_B is the Boltzmann constant.

We plot the change of the magnitude of all the forces in Fig. 7 with $x' = \Delta/(2\sqrt{\epsilon_x})$ and $f' = f + 0.1$ μm, where

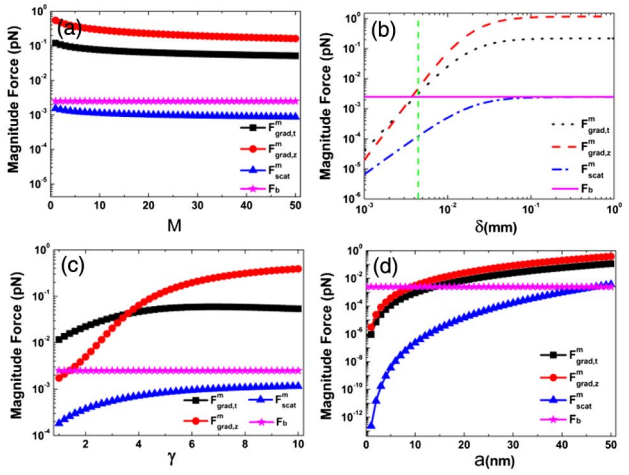

Fig. 7. When $z_1 = 0.1$ μm, the radiation forces F^m_{scat}, $F^m_{\mathrm{grad},t}$, $F^m_{\mathrm{grad},z}$ produced by partially coherent multi-REGBs depend on (a) the initial beam index M with $\delta = 0.1$ mm and $\gamma = 6$, (b) the coherence width δ with $M = 30$ and $\gamma = 6$, (c) the elliptical ratio γ with $M = 30$ and $\delta = 0.1$ mm, and (d) the particle radius a with $M = 30$, $\delta = 0.1$ mm, and $\gamma = 6$. F_b is the Brownian force.

$F^m_{\mathrm{grad},t}$ is maximum transverse gradient force, $F^m_{\mathrm{grad},z}$ is maximum longitudinal gradient force, and F^m_{scat} is maximum scattering force. In Fig. 7(a), the longitudinal gradient force is much bigger than the Brownian motion. In Fig. 7(b), it is found that the particle can be stably trapped when $\delta > 0.005$ mm, but if δ is too small, the Brownian force will be too strong. In Fig. 7(c), the longitudinal gradient force will be bigger than the transverse gradient force while $\gamma > 4$, and the longitudinal gradient force is always bigger than the Brownian force. In Fig. 7(d), it is found that the particle can be stably trapped while 14 nm $< a <$ 50 nm, but when a is too small, the disturbance is mainly from the Brownian motion. However, when a is greater than 45 nm, the disturbance of the Brownian force equals the scattering force. The particle can be stably trapped while 46 nm $< a <$ 50 nm for $\gamma = 1$, 33 nm $< a <$ 50 nm for $\gamma = 2$, and 15 nm $< a <$ 50 nm for $\gamma = 8$. So we can conclude that as γ increases, the radius range of the trapped particle increases.

In conclusion, we investigate the CSD of the partially coherent multi-REGBs that propagate through a focusing optical system, and study the radiation force on a Rayleigh dielectric sphere induced by focused partially coherent multi-REGBs. The partially coherent multi-REGBs rotate while propagating, and the force scope changes. The rotational nature of these beams is interesting for rotating trapped particles. We find that we can increase the transverse and the longitudinal trapping ranges at the focal plane by increasing the beam index M, or by decreasing the correlation width δ. As the elliptical ratio γ increases, the radius range of the trapped particle increases. For oval particles, we can adjust the size of forces in some directions by changing the elliptical ratio of the elliptical beams, which ordinary Gaussian beams cannot do. When comparing the Gaussian beams, it is clear that the partially coherent multi-REGBs have better applications in operating flexibility.

This work was supported by the National Natural Science Foundation of China (Nos. 11374108, 10904041, and 11374107), the Foundation for the Author of Guangdong Province Excellent Doctoral Dissertation (No. SYBZZXM201227), and the Foundation of Cultivating Outstanding Young Scholars ("Thousand, Hundred, Ten" Program) of Guangdong Province in China. Support was also provided by the CAS Key Laboratory of Geospace Environment, University of Science and Technology of China.

References

1. A. Goncharenko, Y. Logvin, A. Samson, and P. Shapovalov, Opt. Commun. **81**, 225 (1991).
2. D. Deng, X. Peng, C. Chen, and B. Chen, J. Korean Phys. Soc. **66**, 774 (2015).
3. D. Deng, Opt. Commun. **285**, 3976 (2012).
4. T. Alieva, E. Abramochkin, A. Asenjo-Garcia, and E. Razueva, Opt. Express **18**, 3568 (2010).
5. X. Peng, C. Chen, Bo Chen, and D. Deng, Chin. Phys. B **24**, 124201 (2015).
6. J. Arnaud and H. Kogelnik, Appl. Opt. **8**, 1687 (1969).
7. A. Goncharenko, *Gaussian Light Beams* (Nauka i tehnika, 1977).
8. D. Liu, H. Wang, Y. Wang, and H. Yin, Opt. Laser Technol **73**, 12 (2015).
9. D. Deng and Q. Guo, Phys. Rev. E **84**, 046604 (2011).
10. A. Ashkin, J. Dziedzic, J. Bjorkholm, and S. Chu, Opt. Lett. **11**, 288 (1986).
11. A. Ashkin, J. Dziedzic, and T. Yamane, Nature **330**, 769 (1987).
12. A. Ashkin, IEEE J. Sel. Top. Quant. **6**, 841 (2000).
13. Y. Harada and T. Asakura, Opt. Commun. **124**, 529 (1996).
14. J. Shu, Y. Chen, and J. Pu, J. Opt. Soc. Am. A **30**, 916 (2013).
15. S. Wang and C. Chan, Nat. Commun. **5**, 1 (2014).
16. X. Liu and D. Zhao, Appl. Opt. **53**, 3976 (2014).
17. H. Yu and W. She, J. Opt. Soc. Am. A **32**, 90 (2015).
18. M. Zhong, X. Wang, J. Zhou, Z. Wang, and Y. Li, Chin. Opt. Lett. **12**, 011403 (2014).
19. A. Ashkin and J. Dziedzic, Science **235**, 1517 (1987).
20. J. Liphardt, B. Onoa, S. Smith, I. Tinoco, and C. Bustamante, Science **292**, 733 (2001).
21. L. Wang, C. Zhao, L. Wang, X. Lu, and S. Zhu, Opt. Lett. **32**, 1393 (2007).
22. M. Bhattacharya and P. Meystre, Phys. Rev. Lett. **99**, 153603 (2007).
23. Y. Jiang, K. Huang, and X. Lu, Opt. Express **19**, 9708 (2011).
24. Z. Liu and D. Zhao, Opt. Express **20**, 2895 (2012).
25. L. Mandel and E. Wolf, *Optical Coherence and Quantum Optics* (Cambridge University Press, 1995).
26. C. Zhao, Y. Cai, X. Lu, and H. Eyyuboğlu, Opt. Express **17**, 1753 (2009).
27. F. Gori and M. Santarsiero, Opt. Lett. **40**, 1587 (2015).
28. G. Zhang, X. Lu, S. Zhou, W. Ma, and J. Zhu, Chin. Opt. Lett. **12**, S11401 (2014).
29. E. Wolf, *Introduction to the Theory of Coherence and Polarization of Light* (Cambridge University Press, 2007).
30. A. Siegman, *Lasers* (University Science Books, 1986).
31. K. Okamoto and S. Kawata, Phys. Rev. Lett. **83**, 4534 (1999).